J. Inst. Eng. India Ser. B (June 2022) 103(3):721–736
https://doi.org/10.1007/s40031-021-00688-1

ORIGINAL CONTRIBUTION

An Effect of Machine Learning Techniques in Electrical Load forecasting and Optimization of Renewable Energy Sources

Saroj Kumar Panda[1] · **Papia Ray**[1]

Received: 9 March 2021 / Accepted: 6 October 2021 / Published online: 4 January 2022

Abstract The prediction of the load from a day ahead or a week ahead is called short-term load forecasting. STLF using ANN gives better results in the power grid because the construction of the model is precise, implementation is easy and the performances are good. The weight consisted neural model is a good whose optimal value was found by using various optimization techniques. This paper explains the effect of different machine learning techniques like genetic algorithm, particle swarm optimization, autoregressive integrated moving average, empirical mode decomposition-particle swarm optimization-adaptive network-based fuzzy inference system in STLF and fuzzy logy for the optimization of renewable energy sources, i.e. solar and wind which is also used for the training of the artificial neural network with the silent effect of backpropagation. The study of different machine learning techniques presented their ability to work to produce the results and their extended application in STLF. From the simulation results, we got an empirical mode decomposition-particle swarm optimization-adaptive network-based fuzzy interference system that provides minor error, which is very much permissible compared to other techniques.

Keywords
Autoregressive integrated moving average (ARIMA) · Empirical mode decomposition-particle swarm optimization-adaptive network-based fuzzy inference system (EMD-PSO-ANFIS) · Short-term load forecasting (STLF) · Renewable energy source (RES)

✉ Papia Ray
papiaray_ee@vssut.ac.in

[1] Department of Electrical Engineering, Veer Surendra Sai University of Technology, Burla, India

Introduction

The power systems are performing good works with STLF. Generally, the models adopted for STLF are working with past climate situations, and the previous load demand datasets knowledge is using for load forecasting (LF). These types of forecasts are used to predict load in a short interval of time, and the prediction of the load is one day in advance. The prediction of load for long time duration will find in mid-term as well as long-term forecasts. But mid-term and long-term forecasts will less consider in the power system due to errors in propagation. Therefore, the exact load determination will impact the maintenance and cost of the grid for electricity production. So, the same load determination is essential in STLF for removing continuous variation in the power system, which causes irregularity of the power supply. The energy management system (EMS) performs its excellent work with STLF because work performance is checked on a chart basis like every day or once a week [1–4]. In EMS, it is very significant to maintain the uniqueness between the load and factor, which influences the load because of the calculation of exactness in the load and the fast result in the forecasting [5–8]. So, there are two methods, i.e. old and new techniques, that are approaching in STLF. The different types of ancient techniques are also given the best outcomes in forecasting [9–12]. Like, the applied techniques in load forecasts are regression method [13–16], time series method [17–19], pattern recognition [20], Kalman filters model [21], etc. which are using for the extensive interval of time, and these techniques are depending on the system. These methods are known as traditional, and the STLF brings good results by combining more than one traditional method [22]. The nonlinear system does not work with such conventional methods, and it occurs between load and factors like

climate and period of the day. This non-linear system makes the disturbance in the construction of the model, and new methods like expert system [23], artificial neural network (ANN) dependent techniques [24–26], a fuzzy logic dependent technique [27] and hybrid Kalman filter [28] are bringing good results in STLF as compare to traditional methods.

From the above techniques, ANN is good because it controls the non-linear values present in between the factors controlling the load and load demands. The neural network gives good results over the non-linear loads. The linear or non-linear mathematical function creates the relation between input and output values in ANN. The suitable work of Hopfield and Boltzmann machine, backpropagation, feed-forward or backward model, arrangements of the model and the mapping between units and layer are helped in the construction of the neural network. The backpropagation (BP) is the suitable training technique for ANN with STLF because the availability of input and output data is utilized by it and controls the weight with the help of loss function, also called observable function and supervised learning control this process. Preoperational training does not require unsupervised learning with the neural network. In most of the literature, the stochastic and uncertainty behaviour of photovoltaic (PV) and wind are not mentioned. So, we have given the detailed work of fuzzy logic in renewable energy sources (RES). The same method is applied in [29], where fuzzy regression is developed using the covariance error vector, which is not using the training method. It is affecting the accuracy of the forecasted load. So, this paper uses linear regression with the proposed evolutionary training method for better accuracy in the forecasted load.

The research gap from the above study is:

- The old techniques are bringing poor results in STLF.
- Time consumption is more
- The design of the model for the forecasting is complicated
- The result obtained by the conventional methods is satisfactory.

So, in this, study the research gap is fulfilled by applying the empirical mode decomposition-particle swarm optimization-adaptive network-based fuzzy inference system (EMD-PSO-ANFIS), in STLF which removes the disadvantages of old techniques. In this technique, the time-series data are decomposed by the EMD and PSO technique to optimize the ANFIS model by creating the relationship between the IMF (intrinsic mode function) and the predictor set.

Machine learning techniques

The works of machine learning techniques like GA-ANN, PSO-ANN, ARIMA, EMD-PSO-ANFIS and fuzzy logy for the optimization of RES (Solar-wind-FL) are explained in this study.

Genetic algorithm-based artificial neural network (GA-ANN)

Genetic algorithm (GA) is nature's evaluation process that can globally search in a stochastic approach [30]. The work of GA starts with initialization which includes the random selection and reasonable calculation for chromosomes. The binary encoded and real encoded based on the problem domain are chromosomes. The probability of the crossover and the mutation methods are two critical parameters for suitable solutions in GA. The new solution will continuously produce this process, and it will stop when the GA meets the stopped condition. It includes different features such as:

Coding

The possible answer to the problem representing the parameter is a gene, and the chromosomes will form from the gene. The chromosomes which are encoded into binary alphabets are known as traditional GA code. In place of binary encoding, this paper presents a simple coding scheme. The chromosomes p is formed arbitrarily from the early population. The population size is represented by p.

Weight Extraction

The weight extraction is performed in the chromosome for the regulating of fitness variables. In the chromosome, the characteristics equation is presented by $x_1, x_2, \ldots, x_d \ldots x_L$ and $x_{kd+1}, x_{kd+2}, \ldots, x_{(k+1)d}$ in kth gene ($k \geq 0$). Equations. (1)-(2) give the real weight w_k.

$$w_k = -\frac{x_{kd+2} * 10^{d-2} + x_{kd+3} * 10^{d-3} + \ldots + x_{(k+1)d}}{10^{d-2}} \quad (1)$$

If $0 \leq x_{kd+1} \leq 5$

$$w_k = \frac{x_{kd+2} * 10^{d-2} + x_{kd+3} * 10^{d-3} + \ldots + x_{(k+1)d}}{10^{d-2}} \quad (2)$$

If $5 \leq x_{kd+1} \leq 9$

Fitness Function

The problem dependent and quality of the solution is measured by the fitness function. The fitness function characterised by this manuscript is given by Eq. (3)

$$\text{fitness} = \frac{1}{1 + \text{MAPE}} \tag{3}$$

where MAPE = mean absolute percentage error.

The procedures for GA-based ANN followed by the above steps are.

Stage 1—The population size, length of the chromosome and parameters are initialized.
Stage 2—The fitness value of the individual is calculated by Eq. (3).
Stage 3—The new individual is generated by mutation and crossover process, and the new generation's fitness value is calculated.
Stage 4—The higher fitness value of an individual is calculated by the roulette wheel assortment scheme, which combines the individuals.
Stage 5—The termination condition is checked. If it came, go to step-6; otherwise, repeat Stage 3 and Stage 4.
Stage 6—The optimal individual is obtained, followed by the above steps. So, the ANN is trained with proper weight selection to perform good results in STLF with the BP technique.

In this model, ANN will develop first, then GA is used to optimise the ANN model, as shown in Fig. 1.

Figure 1 explains the following steps:

1) Use the data for the training of ANN.
2) Train the ANN in MATLAB.
3) ANN will determine the fitness function of GA.
4) The fitness value of GA using ANN will consider as a forecasting value.

Particle Swarm Optimization-based Artificial Neural Network (PSO-ANN)

Eberhart and Kennedy have proposed this technique. It has many merits considering an evolutionary computational approach [31]. The flock of birds and a school of fishes are helping in the formation of PSO by its social behaviour. The velocity of own and the velocity of nearer are used to determine the behaviour of each individual in the swarm. The particle reaches a new position from the calculation of the resultant velocity. In a PSO model, the particles are denoted by x_{i1}, L, x_{id}, L, x_{iD} in a D-dimensional problem which consists of m particles and these particles help find the solution of the problem. The particles are upgraded by the position and velocity as given in Eqs. (4)-(5) in a swarm.

$$x_i(t+1) = x_i(t) + v_i(t+1) \tag{4}$$

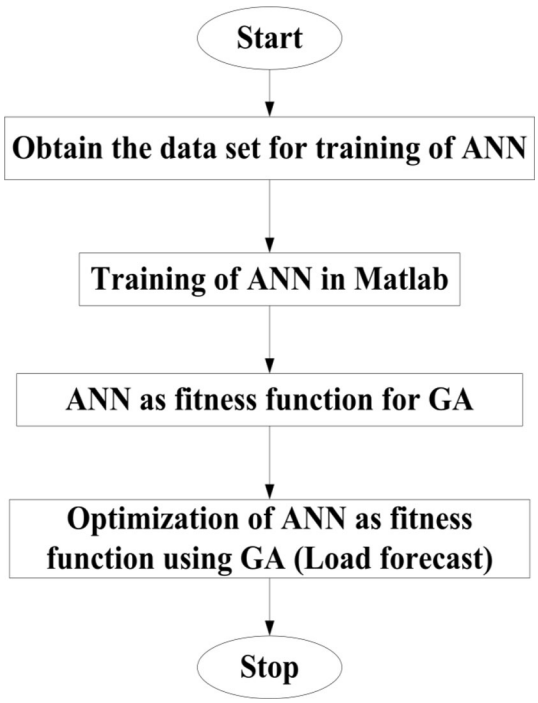

Fig. 1 Schematic of the GA-ANN model

$$v_i(t+1) = wv_i(t-1) + c_1 r_1(localbest(t) - x_i(t-1)) + c_2 r_2(globalbest(t) - x_i(t-1)) \tag{5}$$

where w = inertia weight factor, x = position of particle, v = velocity of particle, r_1, r_2 = random variables which is in the range of 0 to 1, c_1, c_2 = positive acceleration.

The procedures for PSO-based ANN followed by the above steps are.

Stage 1—ANN with BP model is defined for the proposed work with assignment parameters like weight matrix w_0 with the range, learning rate η, particle size, inertia weight factor w, the position of the particle with local optimal *local best* and global optimal *global best*, the positive accelerations c_1, c_2 and at the beginning, the stopping criteria will initialise.
Stage 2—According to the proposed model, the fitness function is given by Eq. (6)

$$\text{fitness} = \frac{1}{1 + \text{MAPE}} \tag{6}$$

MAPE = mean absolute percentage error and offers the fitness value of each particle in a swarm. If the present fitness value is good compared to *local best*, then this fitness value is represented as new loacalbest; otherwise, the earlier value of *local best* is kept.
Stage 3—For the global best ("*global best*") value of the particle, the extreme value of *loacalbest* is selected.

Stage 4—The arbitrary values r1 and r2 are selected, and the position and velocity are updated by Eqs. (4) and (5), respectively.
Stage 5—Set i = i + 1.
Stage 6—Iteration is terminated when the condition is matched, and the *global best* is an optimal solution of the particle; else, it will repeat from Stage 2.

For the load prediction of the system, the ANN model is again optimized by the PSO algorithm, and Fig. 2 gives a schematic diagram of the PSO-ANN structure.

Figure 2 explains that the initialization of the particle is deterring the good results for forecasting in ANN where velocity and position of the particle should be updated using the above equations. Then, the fitness value of the PSO using ANN gives accurate results in the load determination. In this case, the selection of the loop should be correct; otherwise, the loop will increase.

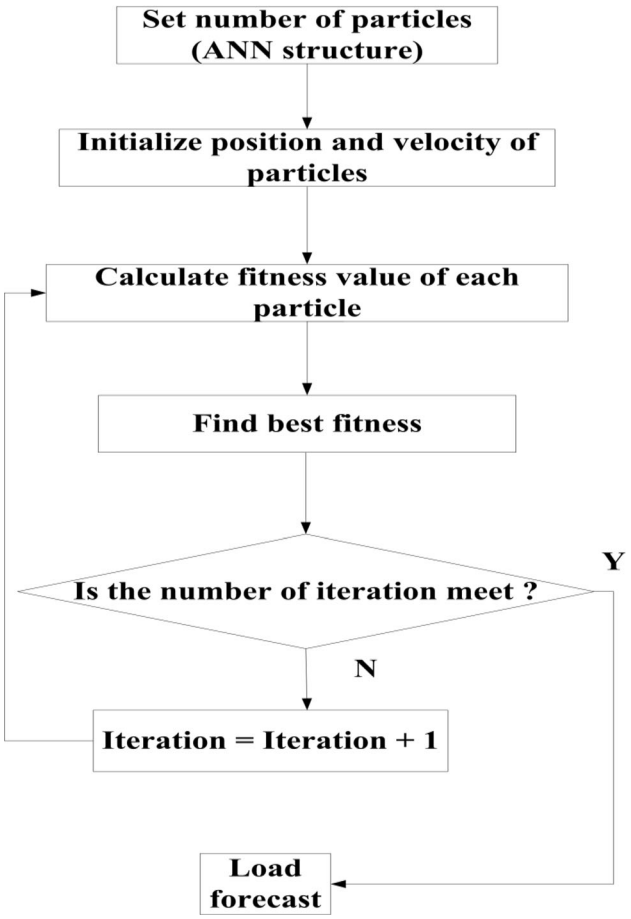

Fig. 2 Schematic of the PSO-ANN model

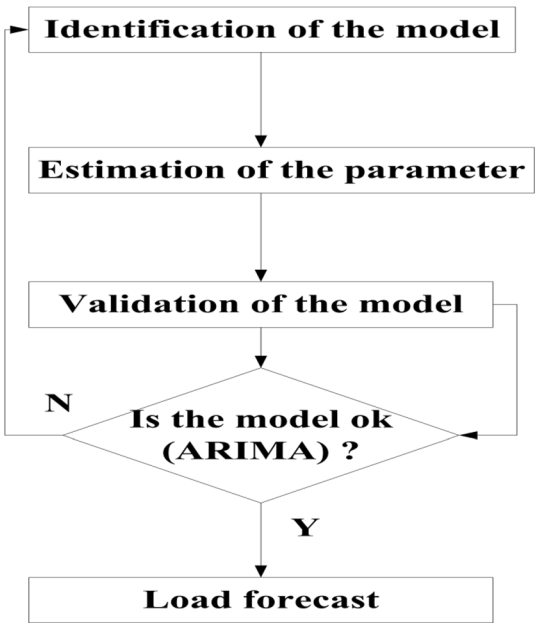

Fig. 3 Schematic of the ARIMA model

Autoregressive Integrated Moving Average Model (ARIMA Model)

When the ARIMA model is considered for other time series as an input, it is called autoregressive moving average with exogenous factor (ARIMAX). It is a dynamic regression discussed by Pankratz in 1991. The important works of ARIMA are the identification of time series model, calculation of parameters, forecasting as well as analysis of ARIMA or ARIMAX related model. The other works of ARIMA are associated with data of seasonal, subset, ARIMA model factor, time series model with constant or interference, ARIMA error with multiple regressions and complicated model with rational transfer function. This model has experienced different improvements throughout the years, and a time-series study considered a standard model for estimation [32]. When the stationary hypothesis of the information is affirmed, different time-series information is clarified with various seasonal (P, Q) and non-seasonal (p, q) requests of ARIMA. The time series takes Eqs. (7)-(11), when $\{y_t | t = 1, 2,\ldots,T\}$ follows ARIMA (p, d, q)(P, D, Q) with μ as mean,

$$\phi_p(l)\Phi_P(l^s)(1-l)^d(1-l^s)^D y_t = \theta_q(l)\Theta_Q(l^s)\varepsilon_t \quad (7)$$

where y_t = At time t (t = 1,2,…., T), the actual value of peak demand (in kilowatts), ε_t = white noise random errors

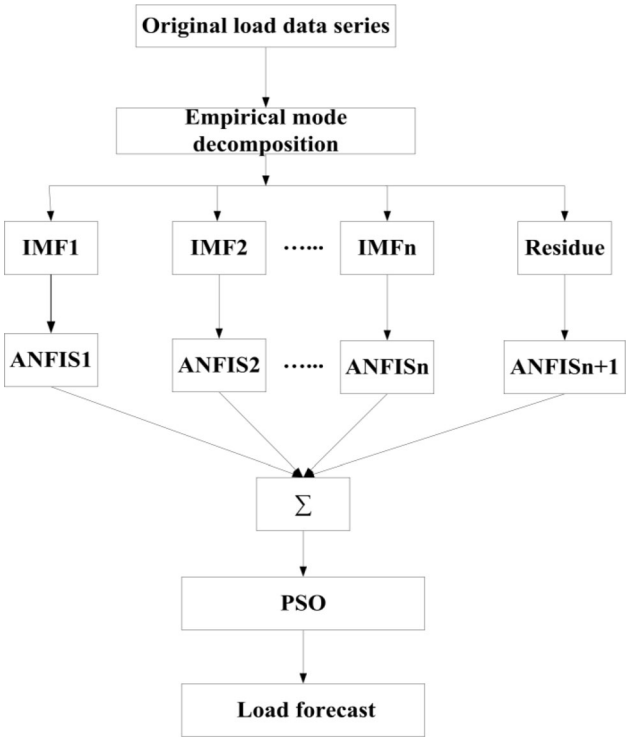

Fig. 4 Schematic of the EMD-PSO-ANFIS model

at t, with the constant variance of $\sigma 2$, zero mean and p, d, and q are orders of the model in integers, $(1 - l)d$ as well as $(1 - l^s)D$ = non-seasonal and seasonal difference operators of order d and D, respectively, s = seasonal cycle.

$$\phi_p(l) = 1 - \phi_1 l - \ldots - \phi_p l^p \tag{8}$$

where p = autoregressive polynomial of non-seasonal.

$$\theta_q(l) = 1 - \theta_1 l - \ldots - \theta_q l^q \tag{9}$$

where q = moving average polynomial of non-seasonal.

For the operation of seasonal,

$$\Phi_P(l^s) = 1 - \Phi_1 l^s - \ldots - \Phi_P l^{Ps} \tag{10}$$

where P = degree of the seasonal autoregressive polynomial

$$\Theta_Q(l^s) = 1 - \Theta_1 l^s - \ldots - \Theta_Q l^{Qs} \tag{11}$$

where Q = degree of the seasonal moving average polynomial.

The load is forecasting with the ARIMA technique by the above equations, as shown in Fig. 3.

Figure 3 explains that the ARIMA technique should be utilized with the load which will forecast. The parameters which are discussed in the above equation will help in the work of ARIMA for the forecast of the load with checking of the model.

Empirical Mode Decomposition-Particle Swarm Optimization-Adaptive Network-Based Fuzzy Inference System Model (EMD-PSO-ANFIS Model)

The proposed strategy associates EMD preprocessing [33–36] to deteriorate the unique time series data and tune the parameters of an ANFIS model for every component; PSO helps. For every subsequent signal component such as IMF, including residues, an early ANFIS model is created. At first, the customizable parameters are haphazardly introduced. After that, during the training procedure, parameters are improved utilizing the PSO. The ANFIS model creates RMSE of the residuals, which are used to limit fitness function.

The following stages explain the complete explanation of the hybrid modelling method.

Stage 1—Raw data series decomposition utilizing EMD: The disintegration of the signal into a limited set of intrinsic mode functions (IMFs). The training dataset is set up for every component.

Stage 2—Initialize FIS structure: An early fuzzy inference system (FIS) is created for every signal from the information speaking of the equivalent IMF utilizing fuzzy c-means (FCM) grouping. The used input

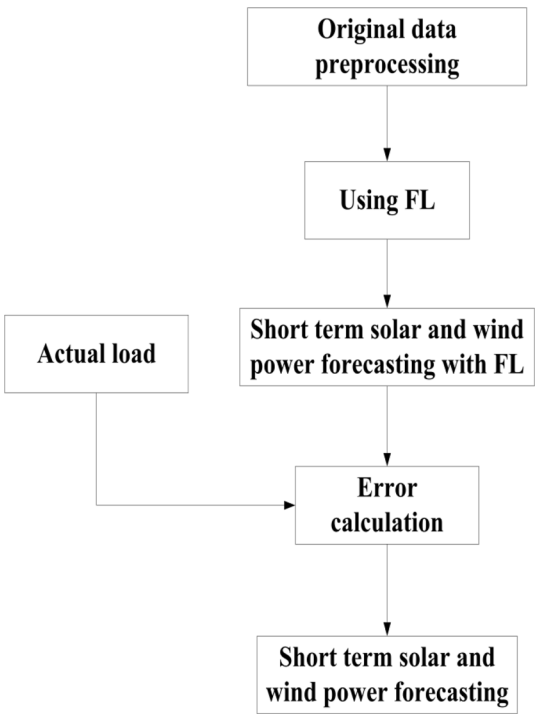

Fig. 5 Schematic of the solar-wind-FL model

Table 1 Comparisons of actual load and the forecasted load of the different models

Time (h)	Actual load (MW)	Forecasted load (MW)					
		BP	GA-ANN	PSO-ANN	ARIMA	EMD-PSO-ANFIS (proposed one)	Solar-wind-FL
1	943	920	980	980	890	948	950
2	914	900	940	940	930	914	915
3	907	890	890	900	1020	913	915
4	875	860	890	900	1060	870	875
5	873	870	860	890	1070	870	880
6	872	860	890	900	1100	870	881
7	931	900	960	955	1125	931	930
8	976	1000	1040	1040	1130	970	980
9	1062	1080	1070	1090	1135	1062	1060
10	1144	1170	1140	1155	1100	1144	1150
11	1213	1240	1160	1190	1070	1213	1220
12	1263	1270	1210	1250	1095	1260	1270
13	1231	1250	1205	1245	1120	1231	1240
14	1196	1200	1160	1195	1130	1196	1200
15	1150	1180	1140	1155	1125	1150	1140
16	1190	1210	1190	1220	1123	1190	1195
17	1212	1200	1240	1220	1120	1212	1213
18	1231	1250	1240	1225	1110	1231	1230
19	1223	1233	1240	1227	1070	1220	1225
20	1228	1270	1200	1240	1025	1225	1230
21	1245	1240	1210	1248	980	1243	1240
22	1317	1330	1290	1330	955	1310	1315
23	1214	1230	1200	1245	925	1213	1215
24	1081	1110	1100	1105	923	1081	1080

membership functions (MF) is triangular when the membership function is linear in output.

Stage 3—Introductory swarm generation: With positions $S_{n,m} \in$ [Smin, Smax], an early swarm S of N vectors having M length individually is haphazardly created. n = 1,2,3… N and m = 1,2,3… M. The PSO has population size N, whereas the ANFIS model contains the number of the parameter is M. Each particle's speed is zero in early stage. In contrast, the swarm cost is infinity universally.

Stage 4—Update of particles' position and speed: On particles of the past generation position and speed update methods as Eqs. (4) and (5) are applied to create particles of another generation. The updated value of inertia weight is given in Eq. (12). The ANFIS structure is trained by using parameters of the PSO algorithm in this study.

Table 2 Estimation of models through preparing period

Technique	RMSE	MAE	NMAE	MAPE
BP	19.96	17.75	82.27	1.43
GA-ANN	206.17	27.16	7.89	1.88
PSO-ANN	213.86	16.95	8.78	39.41
ARIMA	450.31	140.83	8.64	12.58
EMD-PSO-ANFIS (proposed one)	3	1.91	0.4	0.85
Solar-wind-FL	5.15	4.08	83.16	0.34

Table 3 Estimation of different approaches

Metric	Technique	Average
RMSE	BP	4.12
	GA-ANN	24.43
	PSO-ANN	29.69
	ARIMA	163.50
	EMD-PSO-ANFIS(proposed one)	2.73
	Solar-wind-FL	4.59
MAE	BP	17.57
	GA-ANN	21.91
	PSO-ANN	18.87
	ARIMA	149.94
	EMD-PSO-ANFIS (proposed one)	2.99
	Solar-wind-FL	4.01
NMAE	BP	93.03
	GA-ANN	1.87
	PSO-ANN	1.65
	ARIMA	12.58
	EMD-PSO-ANFIS (proposed one)	0.17
	Solar-wind-FL	89.03
MAPE	BP	1.07
	GA-ANN	2.21
	PSO-ANN	1.75
	ARIMA	13.59
	EMD-PSO-ANFIS (proposed one)	0.18
	Solar-wind-FL	0.46

$$W = W_{\max} - \frac{W_{\max} - W_{\min}}{it_{\max}} it \tag{12}$$

where W = inertia weight of ANFIS, W_{max} = inertia weight in maximum, W_{min} = inertia weight in minimum, it = iteration number, it_{max} = iteration number in maximum.

Stage 5—ANFIS parameters allotment: To the input and output MF of the ANFIS, iteratively, the factors of a particle are passed. The number of components of every MF, the input dimension, and the MF of the input and output is resolved so that the MFs of the ANFIS can be copied sequentially by the parameters of a particle.

Stage 6—Evaluation of cost function: Every particle's fitness is assessed; individual and worldwide best positions are restructured. If the specific particle's present estimation of the cost function is not as much as that detected up to this point, it is considered a new *loaclbest*. Likewise, the best particle' cost of the present iteration is not as much as that of best accomplished up to this point; the current best position is considered as the new *global best*.

Stage 7—Check convergence: In the stopping criterion, large numbers of iterations are being utilized. If large numbers of iterations aren't got, the algorithm returns to stage 4. Else, it continues to stage 8.

Stage 8—Model extraction: ANFIS model is run by the PSO upgraded parameters. Then, the final model is removed as well, as the training procedure is finished up.

Table 4 Comparison of the proposed model (EMD-PSO-ANFIS) with conventional techniques

Technique	RMSE	MAPE	Average
T-Coupla-IEMD-DBN	392.44	3.44	197.94
Hybrid SVR	73.27	0.91	37.09
EMD-PSO-ANFIS (proposed one)	3	0.85	1.92

Stages 2 through 8 are repeated for every IMF as well as the remainder. Similarly, the specific ANFIS models relating to every IMF are trained and removed. The total estimates are made by adding estimates acquired from each model.

The work of EMD-PSO-ANFIS is explained in Fig. 4.

Figure 4 explains that EMD breaks down the original datasheet of the load. Then, the PSO is applied to the ANFIS structure to design the model with the relation between IMF signal and tested value. At last, all loads will be added for forecasting the load.

Optimization of RES

A Takagi–Sugeno is used to develop the linear membership-based fuzzy rule space [37] because it estimates the non-linear system with different models. This method helps to form separate linear fuzzy subspace by partition space of the input and output variables. Then, the membership function is created by combining linear fuzzy subspace and the number of rules based on fuzzy c-means clustering reduced by the fuzzy partition method.

The stages for this approach are.

Stage 1—Identification of interval: The specific interval bandwidth with forecasting interval and error of fuzzy covariance is determined.

Stage 2—Band interval: The lower value of bandwidth interval indicates the lower value of interval band, and it indicates calculation of the predicted value from actual load missing is less.

Stage 3—Coverage grade: The performance of the forecasted value is determined by coverage grade. The coverage grade is calculated by Eq. (13)

$$\text{Coverage grade} = \frac{1}{N}\sum_{i=1}^{N} K_i \tag{13}$$

where N = number of the time step, K_i = binary operators.

The proposed schematic diagram is explained in Fig. 5.

Figure 5 explains that the original datasheet of the load is pre-processed with FL. Then predicted loads are compared with actual load for error calculation.

Data

To predict Xingtai's 24 h STLF, contextual analysis for Xingtai Power from the Hebei region, China has been done. The hourly and climate data from 10 June 2006 to 30 June 2006 are being utilized for this analysis. The information is partitioned into three sets of data: 10 June to 20 June training, from 21 to 29 June validation and 30 June data as testing. The total load sheet of the Xintai power plant has also been considered in [38].

Performance Evaluations

In this analysis, to assess the prediction precision of the proposed STLF method, various techniques have been used, as in Eqs. (14)-(17) and the techniques are root mean squared error (RMSE), normalized mean absolute error (NMAE), mean absolute error (MAE) and mean absolute percentage error (MAPE).

$$\text{RMSE} = \sqrt{\frac{1}{N}\sum_{i=1}^{N}(l_i - f_i)^2} \tag{14}$$

$$\text{MAE} = \frac{1}{N}\sum_{i=1}^{N}|f_i - l_i| \tag{15}$$

$$\text{NMAE} = \frac{100}{N}\sum_{i=1}^{N}\left(\frac{|f_i - t_i|}{l_m}\right) \tag{16}$$

$$\text{MAPE} = \frac{100}{N}\sum_{i=1}^{N}\frac{|f_i - l_i|}{l_i} \tag{17}$$

where f_i = forecasted load of the ith time-step, l_i = actual load of the ith time-step, l_m = maximum recorded load and N = number of time-steps.

Simulation Results and Discussions

The MATLAB 2015 software is used for the simulation result. The comparisons of actual and forecasted load are explained in Table 1, and the different types of performance evaluation are presented in Tables 2 and 3, respectively. So, the proposed models' results are reasonable compared to other conventional techniques [39, 40], as given in Table 4. The proposed models have brought minor errors in the forecasted loads.

The forecasted load was obtained with the help of the BP, GA-ANN, PSO-ANN, ARIMA, EMD-PSO-ANFIS and Solar-wind-FL models. Then, the accurateness of the forecasted loads is calculated and compared. The immediate adaptive faster learning process is achieved by resilient BP, which is used as the training process of neural networks. The comparison of the forecasted load of the different models and actual load is shown in Figs. 6(a)–6(x).

Figure 6a explains the work of BP in STLF. The BP obtains the forecasted load is suitable for a minor error in STLF. It also helps in the fast training of the ANN.

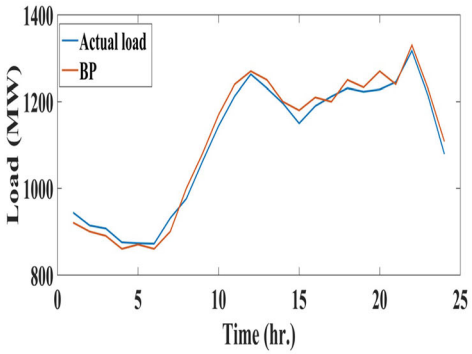

(a) Work of BP

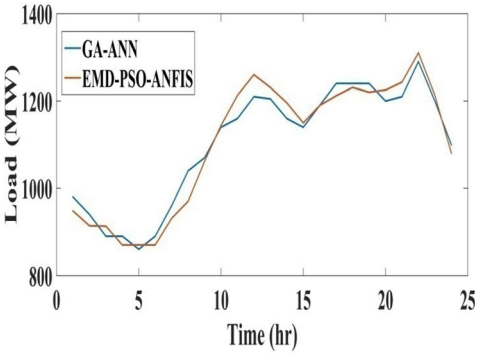

(d) Work of BP and GA-ANN

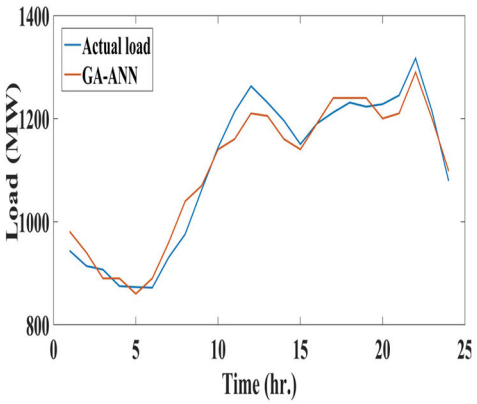

(b) Work of GA-ANN

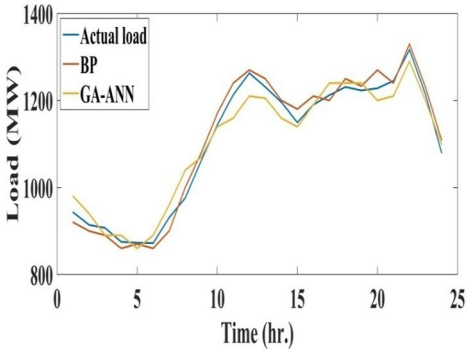

(e) Comparison of actual, BP and GA-ANN loads

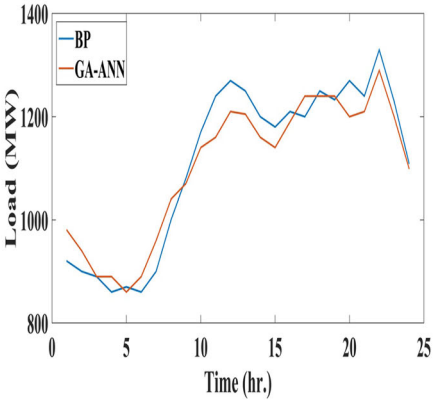

(c) Work of BP and GA-ANN

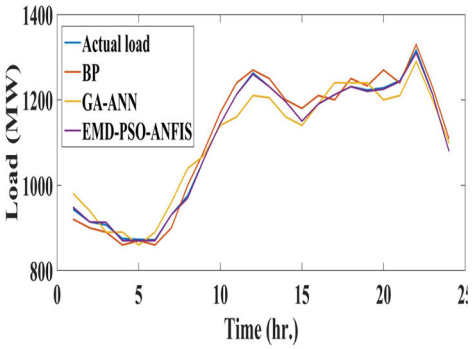

(f) Comparison of actual, BP, GA-ANN and EMD-PSO-ANFIS loads

Fig. 6 **a** Work of BP. **b** Work of GA-ANN. **c** Work of BP and GA-ANN. **d** Work of BP and GA-ANN. **e** Comparison of actual, BP and GA-ANN loads. **f** Comparison of actual, BP, GA-ANN and EMD-PSO-ANFIS loads. **g** Work of PSO-ANN. **h** Work of BP and PSO-ANN. **i** Work of BP and PSO-ANN. **j** Comparison of actual, BP and PSO-ANN loads. **k** Comparison of actual, BP, PSO-ANN, EMD-PSO-ANFIS loads. **l** Work of ARIMA. **m** Work of BP and ARIMA. **n** Work of BP and ARIMA. **o** Comparison of actual, BP and ARIMA loads. **p** Comparison of actual, BP, ARIMA and EMD-PSO-ANFIS loads. **q** Work of EMD-PSO-ANFIS. **r** Work of BP and EMD-PSO-ANFIS. **s** Comparison of actual, BP and EMD-PSO-ANFIS loads. **t** Work of solar-wind-FL. **u** Work of BP and Solar-wind-FL. **v** Work of Solar-wind-FL and EMD-PSO-ANFIS. **w** Comparison of actual, BP and Solar-wind-FL loads. **x** Comparison of actual, BP, Solar-wind-FL and EMD-PSO-ANFIS loads

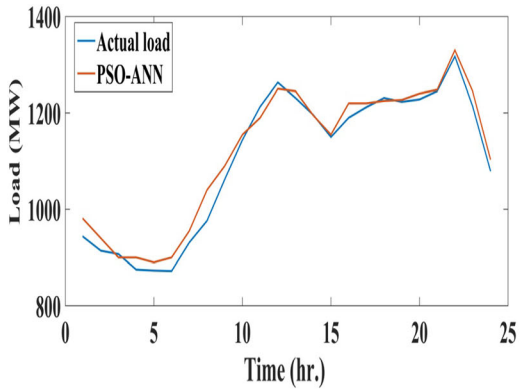

(g) Work of PSO-ANN

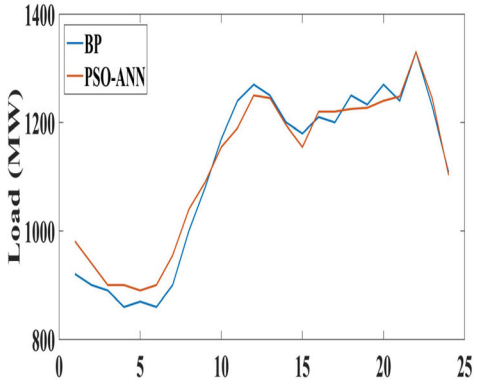

(h) Work of BP and PSO-ANN

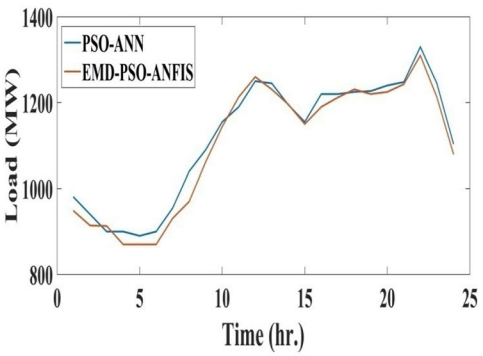

(i) Work of BP and PSO-ANN

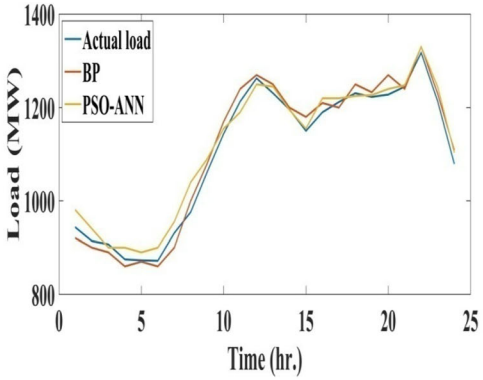

(j) Comparison of actual, BP and PSO-ANN loads

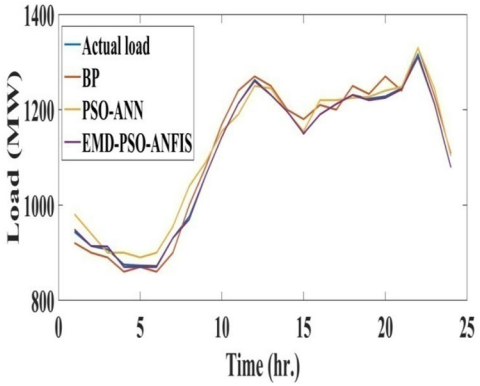

(k) Comparison of actual, BP, PSO-ANN, EMD-PSO-ANFIS loads

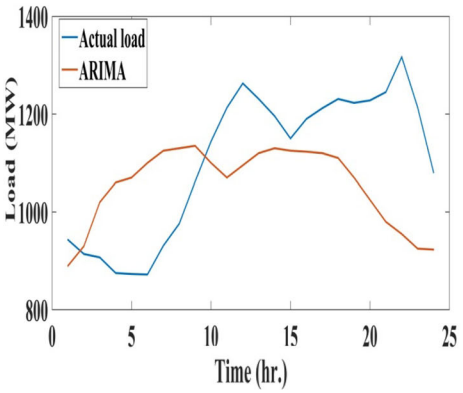

(l) Work of ARIMA

Fig. 6 continued

Figure 6b explains the work of GA-ANN in STLF. The forecasted load is obtained by considering mutation, selection and crossover for a minor error in STLF.

Figure 6c explains the work of BP and GA-ANN in STLF. The forecasted load obtained by the GA-ANN is reasonable as compared to the BP.

Figure 6d explains the work of GA-ANN and EMD-PSO-ANFIS in STLF. The forecasted load obtained by the EMD-PSO-ANFIS is good as compare to the GA-ANN.

Figure 6e explains the comparisons of actual, BP and GA-ANN loads in STLF. The forecasted load obtained by the GA-ANN produces a minor error.

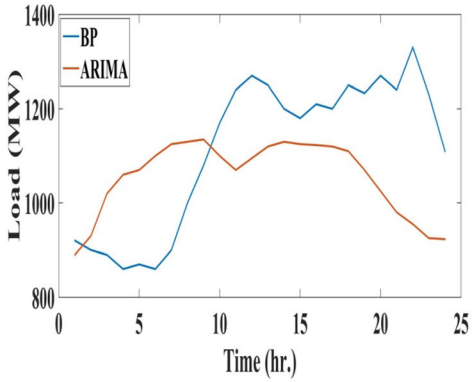

(m) Work of BP and ARIMA

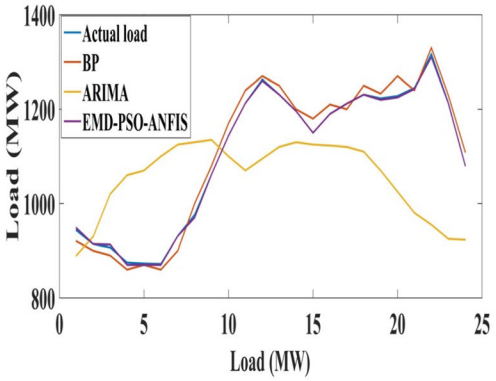

(p) Comparison of actual, BP, ARIMA and EMD-PSO-ANFIS loads

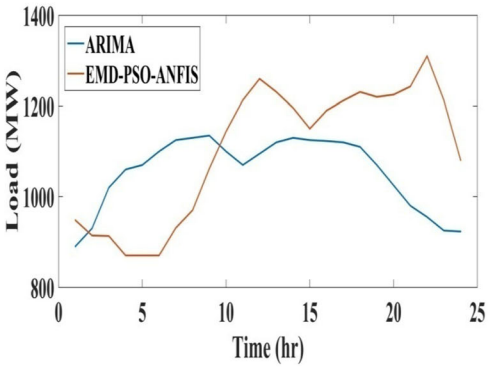

(n) Work of BP and ARIMA

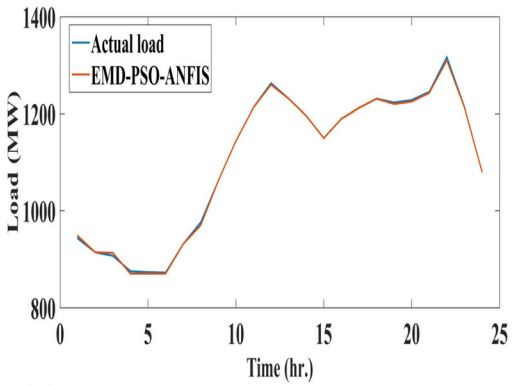

(q) Work of EMD-PSO-ANFIS

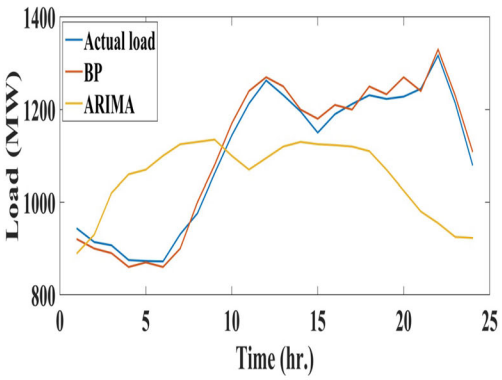

(o) Comparison of actual, BP and ARIMA loads

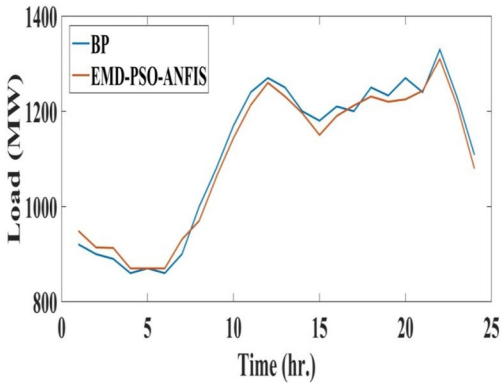

(r) Work of BP and EMD-PSO-ANFIS

Fig. 6 continued

Figure 6f explains the comparison of actual, BP, GA-ANN and EMD-PSO-ANFIS loads in STLF. The forecasted load obtained by the EMD-PSO-ANFIS is good as compare to other techniques.

Figure 6g explains the work of PSO-ANN in STLF. The forecasted load is obtained by the updated velocity and position of the particle for a minor error in STLF.

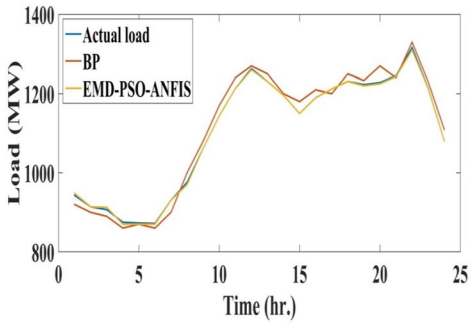

(s) Comparison of actual, BP and EMD-PSO-ANFIS loads

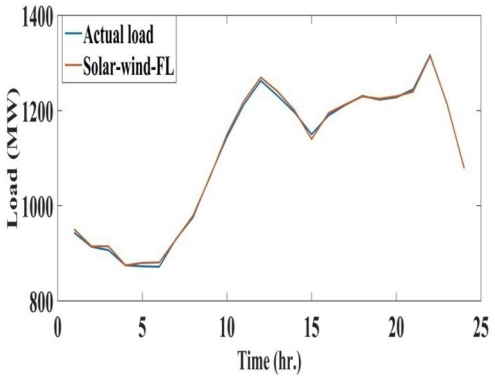

(t) Work of Solar-wind-FL

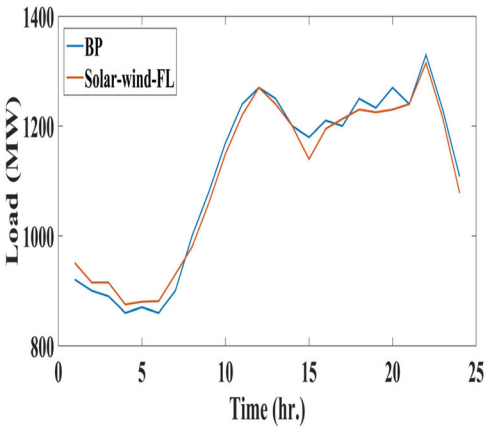

(u) Work of BP and Solar-wind-FL

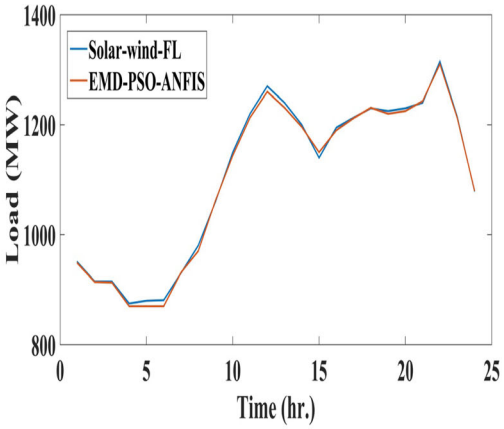

(v) Work of Solar-wind-FL and EMD-PSO-ANFIS

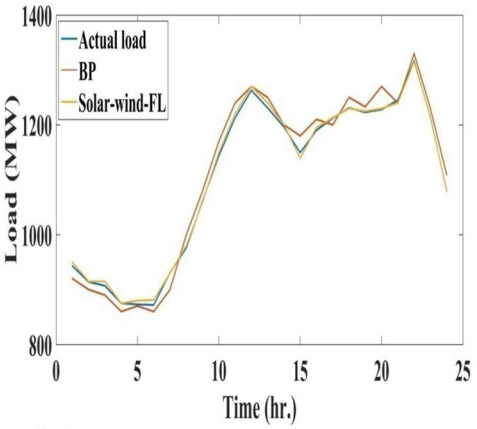

(w) Comparison of actual, BP and Solar-wind-FL loads

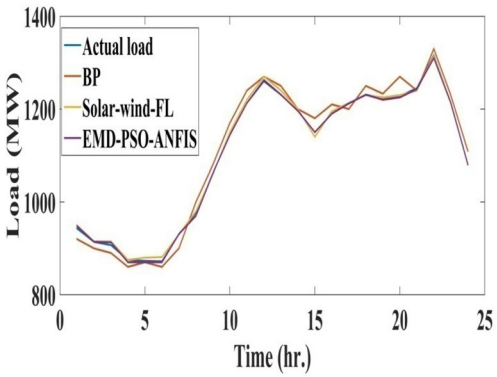

(x) Comparison of actual, BP, Solar-wind-FL and EMD-PSO-ANFIS loads

Fig. 6 continued

Figure 6h explains the work of BP and PSO-ANN in STLF. The forecasted load obtained by the PSO-ANN is reasonable as compared to the BP.

Figure 6i explains the work of PSO-ANN and EMD-PSO-ANFIS in STLF. The forecasted load obtained by the EMD-PSO-ANFIS is good as compare to the PSO-ANN.

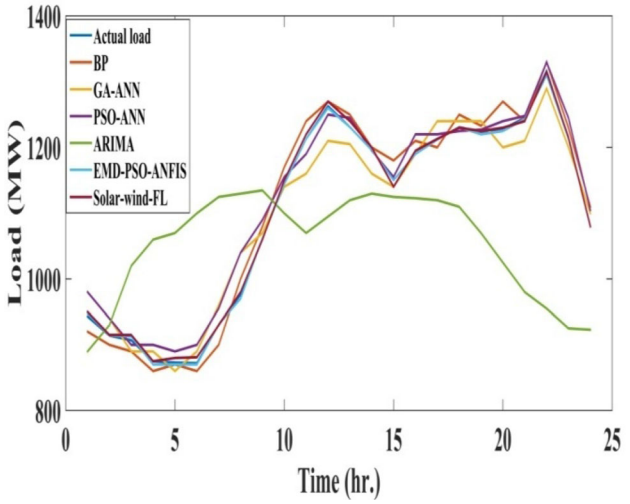

Fig. 7 Graph of the actual load, BP, GA-ANN, PSO-ANN, ARIMA, EMD-PSO-ANFIS and solar-wind-FL models

Figure 6j explains the comparisons of actual, BP and PSO-ANN loads in STLF. The forecasted load obtained by the PSO-ANN produces a minor error.

Figure 6k explains the comparison of actual, BP, PSO-ANN and EMD-PSO-ANFIS loads in STLF. The forecasted load obtained by the EMD-PSO-ANFIS is good as compare to other techniques.

Figure 6l explains the work of ARIMA in STLF. The forecasted load is obtained by considering seasonal and non-seasonal parameters for a minor error in STLF.

Figure 6m explains the work of BP and ARIMA in STLF. The forecasted load obtained by the ARIMA is reasonable as compared to the BP.

Figure 6n explains the work of ARIMA and EMD-PSO-ANFIS in STLF. The forecasted load obtained by the EMD-PSO-ANFIS is good as compare to the ARIMA.

Figure 6o explains the comparisons of actual BP and ARIMA loads in STLF. The forecasted load obtained by the ARIMA produces a minor error.

Figure 6p explains the comparison of actual BP, ARIMA and EMD-PSO-ANFIS loads in STLF. The forecasted load obtained by the EMD-PSO-ANFIS is good as compare to other techniques.

Figure 6q explains the work of EMD-PSO-ANFIS in STLF. The forecasted load is obtained by considering intrinsic mode functions (IMFs) for a minor error in STLF.

Figure 6r explains the work of BP and EMD-PSO-ANFIS in STLF. The forecasted load obtained by the EMD-PSO-ANFIS is reasonable as compared to BP.

Figure 6s explains the comparison of actual BP and EMD-PSO-ANFIS in STLF. The forecasted load obtained by the EMD-PSO-ANFIS produces good results.

Figure 6t explains the work of Solar-wind-FL in STLF. The forecasted load is obtained by the consideration of the member function for a minor error in STLF.

Figure 6u explains the work of BP and Solar-wind-FL in STLF. The forecasted load obtained by the solar wind-FL is reasonable as compared to BP.

Figure 6v explains the work of Solar-wind-FL and EMD-PSO-ANFIS in STLF. The forecasted load obtained by the EMD-PSO-ANFIS is good as compare to Solar-wind-FL.

Figure 6w gives a comparison of actual, BP and Solar-wind-FL loads and it can be observed that the solar-wind-FL gives a close relation with the actual values.

Figure 6x explains the comparison of actual, BP, Solar-wind-FL-BP and EMD-PSO-ANFIS loads in STLF. The forecasted load obtained by the EMD-PSO-ANFIS is good as compare to other techniques.

Table 1 gives the comparison of the forecasted load with the actual load by using different approaches. The proposed work (EMD-PSO-ANFIS) gives accurate forecasted load as compared to the other methods.

Table 2 gives a comparison of the errors by different approaches. The proposed work (EMD-PSO-ANFIS) gives minor errors as compared to the other methods.

Table 3 explains the superiority of the EMD-PSO-ANFIS demonstrated by the test results over the other approaches. The outcomes show that the average value of RMSE, MAE, NMAE and MAPE of the EMD-PSO-ANFIS over the test period are 2.73, 2.99, 0.17 and 0.18, respectively.

Table 4 explains the proposed models give minor errors using STLF, which helps to bring accurateness and stability of the load in the grid.

Figure 7 explains that the curve of EMD-PSO-ANFIS has delivered an exact estimate with considerable execution improvements over the other curves like BP, GA-ANN, PSO-ANN, ARIMA and Solar-wind-FL models with respect to actual load.

Forecasting Load with Real-Time Data

The real-time data are considered from the Hirakud power plant, Odisha, and the forecasted load gives different models in Table 5 compared to Table 1. The hourly and climate data from 1 May 2015 to 31 May 2015 are being utilized for this analysis. The information is partitioned into three sets of data: 1 May to 10 May training, from 11 to 30 May validation and 31 May data as testing. The total load sheet of the Hirakud power plant has also considered.

Table 5 gives the comparison of the forecasted load with the actual load by using different approaches. The proposed

Table 5 Forecasted load of different models with real-time data

Time (h)	Actual load (MW)	Forecasted load (MW)					
		BP	GA-ANN	PSO-ANN	ARIMA	EMD-PSO-ANFIS (proposed one)	Solar-wind-FL
1	192	110	125	190	200	191	180
2	220	170	210	213	240	220	200
3	240	200	210	220	225	235	211
4	252	190	230	240	235	248	280
5	256	150	210	230	250	255	290
6	252	170	180	200	230	240	230
7	240	180	210	220	235	238	250
8	726	657	700	720	750	725	730
9	792	700	730	710	735	780	800
10	858	800	830	835	860	856	850
11	924	889	900	920	915	924	930
12	990	800	900	930	940	989	1000
13	1056	1000	1010	1030	1040	1055	1200
14	1122	1180	1100	1110	1120	1196	1200
15	1188	1230	1140	1155	1125	1122	1195
16	1254	1200	1220	1230	1140	1253	1280
17	1320	1180	1300	1310	1315	1319	1330
18	1386	1300	1316	1340	1350	1385	1390
19	1452	1400	1410	1420	1440	1450	1488
20	1318	1580	1500	1511	1515	1518	1540
21	1284	1500	1400	1300	1200	1280	1510
22	1150	1400	1300	1200	1190	1150	1200
23	1130	1350	1200	1120	1120	1180	1180
24	1048	1000	1140	1110	1100	1048	1200

work (EMD-PSO-ANFIS) gives accurate forecasted load as compared to the other methods.

Figure 8 explains that the curve of EMD-PSO-ANFIS with real-time data has delivered an exact estimate with considerable execution improvements over the other curves like BP, GA-ANN, PSO-ANN, ARIMA and Solar-wind-FL models with respect to actual load.

Comparison of Conventional Methods for Load Forecasting

Traditional methods like ANN, linear regression (LR) and FL are used for load forecasting, and these methods have explained the work of each model for the forecasted load as given in Table 6. The conventional methods are also compared with the proposed method.

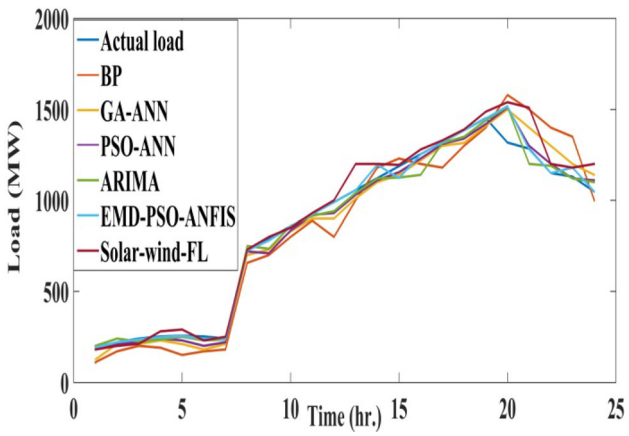

Fig. 8 Graph of the actual load, BP, GA-ANN, PSO-ANN, ARIMA, EMD-PSO-ANFIS and solar-wind-FL models

Table 6 Comparison of different schemes for forecasted load

Scheme	Use of methods	Accuracy testing (%)
[5]	ANN	91
[8]	LR	81
[37]	FL	85
Proposed method	EMD-PSO-ANFIS	99

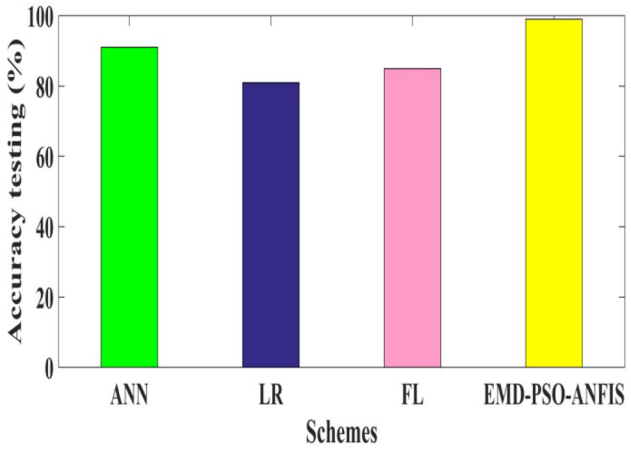

Fig. 9 Accuracy testing of ANN, LR, FL and EMD-PSO-ANFIS

Table 6 gives the comparison of work published by other researcher's with the proposed technique in this paper. The accuracy of proposed one is 99% as compared to other schemes and thus recommended as a forecasting tool.

Figure 9 explains the accuracy testing of different conventional methods with the proposed technique. The accuracy testing of EMD-PSO-ANFIS is 99% which is best as compared to the other methods.

Conclusion

The working of STLF with various models is the main objective of the work. These models are working in a computational intellectual way. The calculation of the exactness of the load affects the transmission, distribution, operation, maintenance and cost of electricity. The analysis of the exact load for the power plant is complicated. So, we are using different techniques in this manuscript. The work of EMD-PSO-ANFIS is better than GA-ANN, PSO-ANN, ARIMA and Solar-wind-FL techniques. GA-ANN has brought good results in forecasted load, but the mutation and crossover process for the new generation makes the loss of characteristics in the chromosome. While PSO has good results, compare to GA with updating of velocity and position of the particle. But compare to GA, PSO, the ARIMA has a high error which is a good technique for time series data, and Solar-wind-FL tries to bring good results in the grid. The proposed hybrid technique EMD-PSO-ANFIS is good compared to the GA, PSO, ARIMA and Solar-wind-FL approach because the selection of the factors is not more impact the forecasted results. So, it is a good technique compare to other processes.

Funding The authors declare that they have no any funding source for doing this research work.

Declarations

Conflict of interest The authors have no conflict of interest.

References

1. J.C. López, M.J. Rider, Q. Wu, Parsimonious short-term load forecasting for optimal operation planning of electrical distribution systems. IEEE Trans. Power Syst. **34**(2), 1427–1437 (2019)
2. S. Fan, R.J. Hyndman, Short-term load forecasting based on a semi-parametric additive model. IEEE Trans. Power Syst. **27**, 134–141 (2012)
3. M.Q. Raza, A. Khosravi, A review on artificial intelligence-based load demand forecasting techniques for smart grid and buildings. Renew. Sustain. Energy Rev. **50**, 1352–1372 (2015)
4. T. Hong, S. Fan, Probabilistic electric load forecasting: a tutorial review. Int. J. Forecast. **32**(3), 914–938 (2016)
5. N.M. Pindoriya, S.N. Singh, S.K. Singh, Forecasting of short-term electric load using application of wavelets with feed-forward neural networks. Int. J. Emerg. Electr. Power Syst. **11**(1), 1–24 (2010)
6. S. Mohajeryami, M. Doostan, S. Moghadasi, P. Schwarz, Towards the interactive effects of demand response participation on electricity spot market price. Int. J. Emerg. Electr. Power Syst. **18**(1), 158–164 (2017)
7. N. Charlton, C. Singleton, A refined parametric model for short term load forecasting. Int. J. Forecast. **30**(2), 364–368 (2014)
8. S. Haben, G. Giasemidis, A hybrid model of kernel density estimation and quantile regression for gefcom2014 probabilistic load forecasting. Int. J. Forecast. **32**, 1017–1022 (2016)
9. S.K. Panda, P. Ray, D.P. Mishra, Short term load forecasting using metaheuristic techniques. IOP Conf. Ser. Mater. Sci. Eng. **1033**(1), 1–10 (2021)
10. S.K. Panda, P. Ray, D.P. Mishra, An efficient short-term electric power load forecasting using hybrid techniques. Int. J. Comput. Inf. Syst. Ind. Manag. Appl. **12**, 387–397 (2020)
11. S.K. Panda, P. Ray, Analysis and evaluation of two short-term load forecasting techniques. Int. J. Emerg. Electr. Power Syst. (2021). https://doi.org/10.1515/ijeeps-2021-0051
12. A. Bracale, G. Carpinelli, A.D. Fazio, S. Khormali, Advanced Cost-based indices for forecasting the generation of photovoltaic power. Int. J. Emerg. Electr. Power Syst. **15**(1), 77–91 (2014)
13. C. Zhang, H. Wei, X. Zhao, T. Liu, K. Zhang, A Gaussian process regression based hybrid approach for short-term wind speed prediction. Energy Convers. Manag. **126**, 1084–1092 (2016)
14. P. Areekul, T. Senju, H. Toyama, S. Chakraborty, A. Yona, N. Urasaki, P. Mandal, A.Y. Saber, A new method for next-day price forecasting for PJM electricity market. Int. J. Emerg. Electr. Power Syst. **11**(2), 1–21 (2010)

15. X. Liu, A new method to generate daily load scenario of electric vehicle charging station considering time correlation. Int. J. Emerg. Electr. Power Syst. **21**(2), 252–267 (2020)
16. C.N. Bhende, S. Panda, S. Mishra, A. Narayanan, T. Kaipia, J. Partanen, Optimal power flow management and control of grid-connected photovoltaic-battery system. Int. J. Emerg. Electr. Power Syst. **20**(5), 1–16 (2019)
17. B. Zhang, J.L. Wu, P.C. Chan, A multiple time series-based recurrent neural network for short-term load forecasting. Soft Comput. **22**, 4099–4112 (2018)
18. B. Pamulaparthy, K.S. Swarup, R. Kommu, Load segmentation for convergence of distribution automation and advanced metering infrastructure systems. Int. J. Emerg. Electr. Power Syst. **15**(6), 607–619 (2014)
19. S.K. Soonee, S.S. Barpanda, M. Joshi, N. Mishra, V. Bhardwaj, Point of Connection transmission pricing in India. Int. J. Emerg. Electr. Power Syst. **14**(1), 9–16 (2013)
20. D. Couto, C. Zipfel, Regulation of pattern recognition receptor signalling in plants. Nat. Rev. Immunol. **16**, 537–552 (2016)
21. S. Sharma, A. Majumdar, V. Elvira, E. Chouzenou, Blind Kalman filtering for short-term load forecasting. IEEE Trans. Power Syst. **35**(6), 4916–4919 (2020)
22. P. Zeng, M. Jin, M.F. Elahe, Short-term power load forecasting based on cross multi-model and second decision mechanism. IEEE Access. **8**, 184061–184072 (2020)
23. P. Singh, Indian summer monsoon rainfall (ISMR) forecasting using time series data: A fuzzy-entropy-neuro based expert system. Geosci. Front. **9**(4), 1243–1257 (2018)
24. W. Kong, Z.Y. Dong, Y. Jia, D.J. Hill, Y. Xu, Y. Zhang, Short-term residential load forecasting based on LSTM recurrent neural network. IEEE Trans. Smart Grid. **10**(1), 841–851 (2019)
25. Z. Deng, B. Wang, Y. Xu, T. Xu, C. Liu, Z. Zhu, Multi-scale convolutional neural network with time-cognition for multi-step short-term load forecasting. IEEE Access. **7**, 88058–88071 (2019)
26. P.M.R. Bento, J.A.N. Pombo, M.R.A. Calado, S.J.P.S. Mariano, Optimization of neural network with wavelet transform and improved data selection using bat algorithm for short-term load forecasting. Neurocomputing **358**, 53–71 (2019)
27. Z.M. Yaseen, I. Ebtehaj, H. Bonakdari, R.C. Deo, A.D. Mehr, W.H.M.W. Mohtar, L. Diop, A. Shafie, V.P. Singh, Novel approach for streamflow forecasting using a hybrid ANFIS-FFA model. J. Hydrol. **554**, 263–276 (2017)
28. H.H.H. Aly, An intelligent hybrid model of neuro wavelet, time series and recurrent Kalman Filter for wind speed forecasting. Sustain. Energy Technol. Assess. **41**, 100802 (2020)
29. D. Sáez, F. Ávila, D. Olivares, C. Cañizares, L. Marin, Fuzzy prediction interval models for forecasting renewable resources and loads in microgrids. IEEE Trans. Smart Grid. **6**(2), 548–556 (2015)
30. S.M.C. Eugenio, F.S. Úbeda, A. Muñoz, Rethinking weather station selection for electric load forecasting using genetic algorithms. Int. J. Forecast. **36**(2), 695–712 (2020)
31. B. Gordan, D.J. Armaghani, M. Hajihassani, M. Monjezi, Prediction of seismic slope stability through a combination of particle swarm optimization and neural network. Eng. Comput. **32**, 85–97 (2016)
32. S. Maldonado, A. González, S. Crone, Automatic time series analysis for electric load forecasting via support vector regression. Appl. Soft Comput. **83**, 105616 (2019)
33. Y.K. Somero, J. Zhang, D. Zheng, EMD-PSO-ANFIS-based hybrid approach for short term load forecasting in microgrids. IET Gen. Trans. Distrib. **14**(3), 470–475 (2020)
34. P. Jiang, F. Liu, Y. Song, A hybrid forecasting model based on date-framework strategy and improved feature selection technology for short-term load forecasting. Energy **119**, 694–709 (2017)
35. N.A. Yahya, R. Samsudin, A. Shabri, Tourism forecasting using hybrid modified empirical mode decomposition and neural network. Int. J. Adv. Soft Comput. Appl. **9**(1), 14–31 (2017)
36. X. Wang, Y. Wang, A Hybrid Model of EMD and PSO-SVR for short-term load forecasting in residential quarters. Math. Problems Eng. **2016**, 1–10 (2016)
37. S.N. Vassilyev, Y.I. Kudinov, F.F. Pashchenko, I.S. Durgaryan, A.Y. Kelina, I.Y. Kudinov, A.F. Pashchenko, Intelligent control systems and fuzzy controllers. I. fuzzy models, logical-linguistic and analytical regulators. Autom. Remote Control. **81**, 171–191 (2020)
38. P. Ray, S.R. Arya, S. Nandkeolyar, Electric load forecasts by metaheuristic based back propagation approach. J. Green Eng. **7**, 61–82 (2017)
39. W. Yang, J. Wang, R. Wang, Research and application of a novel hybrid model based on data selection and artificial intelligence algorithm for short term load forecasting. Entropy **19**(52), 1–27 (2017)
40. M.R. Haq, A.Z. Ni, A new hybrid model for short-term electricity load forecasting. IEEE Access. **7**, 125413–125423 (2019)